Case Studies in Thermal Engineering 77 (2026) 107528

Contents lists available at ScienceDirect

Case Studies in Thermal Engineering

journal homepage: www.elsevier.com/locate/csite

A novel concave-wall absorber for enhanced heat flux distribution and thermal stability in linear Fresnel solar receivers

Salman Brbhan [a,*], Basim Belgasim [b,c], Ahmed Al Mers [d], Zoltán Siménfalvi [a], Zoltán Szamosi [a]

[a] Faculty of Mechanical Engineering and Informatics, University of Miskolc, Miskolc, Hungary
[b] Mechanical Engineering Department, University of Benghazi, Libya
[c] Libyan Authority for Scientific Research, Tripoli, Libya
[d] Abdelmalek Essaâdi University, Tétouan, Morocco

GRAPHICAL ABSTRACT

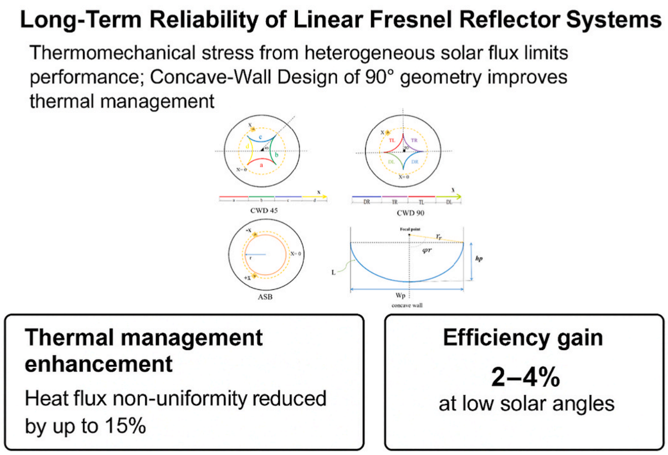

ARTICLE INFO

Keywords:
Linear Fresnel reflectors
Ray tracing
Optical efficiency

ABSTRACT

The long-term reliability of Linear Fresnel Reflector (LFR) systems is critically limited by thermomechanical stress, which arises from heterogeneous solar flux on the receiver tube. To address this challenge, this work investigates the optical performance of two new Concave-Wall Design, of

* Corresponding author.
E-mail address: slmanbarbahan@gmail.com (S. Brbhan).

https://doi.org/10.1016/j.csite.2025.107528
Received 18 August 2025; Received in revised form 21 November 2025; Accepted 6 December 2025
Available online 8 December 2025

Heat flux distribution
Interception ratio
Concentrated solar thermal

45° and 90° orientations, evacuated receivers. A comparative analysis against a conventional circular absorber was conducted using high-fidelity Monte Carlo ray-tracing across diverse geographic and seasonal conditions. The primary finding is that the Concave-Wall Design of 90° orientation geometry provides a substantial enhancement in thermal management; heat flux non-uniformity was reduced by up to 15 %, a result achieved by geometrically dividing the concentrated flux to eliminate damaging hotspots. While optically competitive, the Concave-Wall Design designs also showed a minor efficiency gain (2–4 %) at low solar angles. This study demonstrates that a strategic geometric redesign can solve a key failure mode in linear Fresnel reflector technology, showing that a negligible trade-off in peak optical performance yields a crucial improvement in thermal stability and receiver durability.

1. Introduction

The growing global demand for energy, coupled with the immediate need to mitigate climate change, has intensified the search for sustainable and environmentally benign power generation technologies [1,2]. Among the available options, solar energy stands out as a particularly abundant and promising renewable resource. Within this field concentrating Solar Power (CSP) technologies offer a specific advantage: they convert solar radiation into high-temperature thermal energy, which can then be used directly for industrial processes or dispatched reliably for electricity generation, often facilitated by integrated thermal energy storage [3,4]. Within CSP technologies, linear Fresnel reflector (LFR) systems have attracted increasing attention as a cost-effective alternative to the more established parabolic trough collectors [5,6]. LFRs utilize long rows of relatively flat or slightly curved mirrors to track the sun and focus direct normal irradiance (DNI) onto a fixed, elevated linear receiver. This configuration offers several practical advantages, including simpler mirror manufacturing, reduced land-use requirements, and easier maintenance of the stationary receiver assembly [7,8]. As a result, LFR technology is being explored for a broad range of applications, from utility-scale power plants to industrial heat generation and desalination [9,10].

The fundamental operating principle of an LFR involves the collective focusing of sunlight by multiple mirror rows onto a linear receiver positioned above them. Each mirror row adjusts its tilt angle throughout the day to maintain focus on the receiver as the sun moves across the sky. The receiver assembly typically consists of several key components. At its core is the absorber tube, conventionally a metallic pipe with a circular cross-section, often equipped with a selective coating to maximize solar absorption while minimizing thermal re-radiation losses [11]. This absorber tube is usually enclosed within a glass envelope to reduce convective and radiative heat losses. In many designs, a secondary reflector typically a compound parabolic concentrator (CPC) or a similar non-imaging geometry is placed beneath the absorber to intercept rays that would otherwise miss the tube and redirect them onto the absorber, thereby enhancing the system's optical efficiency [12] This absorber tube is usually enclosed within an evacuated glass envelope to suppress convective heat losses. Often, a secondary reflector, typically a Compound Parabolic Concentrator (CPC) or similar geometry, is placed beneath the absorber tube to capture rays that might otherwise miss the target and redirect them onto the absorber, thereby enhancing the system's optical efficiency [13]. A heat transfer fluid (HTF) flows inside the absorber, collecting the concentrated thermal energy for subsequent use.

Despite the architectural advantages of LFR systems, the performance and long-term reliability associated with the standard circular absorber tube (ASB) configuration face inherent challenges. Optically, LFR systems are susceptible to significant cosine losses, as the effective aperture of the mirror field decreases when the sun is at lower elevation angles (morning, evening, winter months) [14]. Furthermore, the acceptance angle of the receiver system, particularly with a simple cylindrical absorber, can limit its ability to efficiently capture rays reflected from mirrors located far from the receiver's centreline, leading to optical spillage [15].

Beyond optical limitations, the thermal performance of the standard ASB design presents critical issues. Due to the directional nature of the incoming concentrated sunlight, the flux distribution on the surface of the circular absorber is highly non-uniform. The sun-facing side experiences intense peak heat fluxes, while the opposite side receives considerably less radiation. This flux heterogeneity leads to significant circumferential temperature gradients around the absorber tube. Such gradients induce severe thermal stresses within the absorber material and the selective coating, potentially causing deformation, fatigue, cracking, and premature failure, thereby compromising the receiver's durability and operational lifespan [16]. Moreover, localized overheating can degrade the HTF and reduce the overall efficiency of heat transfer compared to more uniform heating [17].

In linear Fresnel reflector (LFR) systems, secondary optics are used to improve the collection, focusing and distribution of radiation. The secondary reflector was optimized using the Bezier-Bernstein method to enhance the optical performance and heat transfer uniformity by 20.5 %, which in turn increased the system efficiency from 61.01 % to 72.84 % [8]. The optical efficiency was boosted by 13 % and the heat flow variation was reduced by 75 % due to the dynamic positioning of the absorber position according to the solar conditions. The weekly adjustments were most effective in not interfering while only causing 2 % efficiency loss [10]. The adaptive design which has been proposed by NREL, out compared conventional CPC, trapezoid, and butterfly designs by flexibly modifying the secondary reflector shape in real time to enhance power production and overall efficiency [11].

As for the types of absorbers, they are divided according to the operating environment and according to the arrangement of the tubes. According to the operating environment, we have the first type called atmospheric absorbers (Non-Evacuated Receivers), which operate at normal atmospheric pressure without removing the surrounding air. They are simpler in design and less expensive, but they suffer from greater heat loss by convection and conduction. They are also used in medium-temperature applications, such as water heating and light industrial processes [12] The second type is called evacuated receivers, which contain a glass tube evacuated of air around the absorber to reduce heat loss through convection. They are characterized by providing higher thermal efficiency, and thus they are applicable to high temperature processes such as steam generation and electrical power generation. It is mainly used in parabolic trough solar collectors or linear Fresnel reflectors [13]. In terms of tube arrangement, the first absorber design is the Single-Tube Receiver that has a single tube placed at the focus of reflector system and has a simple design and easy maintenance but may have uneven heat distribution and is used in linear parabolic mirror systems [18] The Multi-Tube Receiver, however, consists of several tubes disposed in a row to enhance the collection of heat and the rate of energy transport. It reduces the risk of thermal stress and offers increased absorption area that improves the overall performance of the system. It is applied in linear Fresnel mirror (LFR) systems to enhance thermal efficiency and minimize heating variation [19]. The performance can also be enhanced by the integration of a front glass cover to avoid compromising of the absorber by environmental factors such as wind and dust. Moreover, the glass cover minimizes heat loss by radiation by establishing a thermal insulation that prevents heat from escaping to the surrounding air, materials to decrease reflection and increase solar absorption, thus improving the conversion of heat.

Practical experiences, such as those documented with the LFR1832 prototype system at the Cyprus Institute, have highlighted these challenges, where managing high flux peaks and associated thermal stresses proved problematic [16,17]. In response, the research community has explored several advanced solutions. One prominent approach involves optimizing or dynamically adapting the secondary reflector, such as using Bezier-Bernstein methods [18] or adaptive designs proposed by NREL [11], to improve flux uniformity. While effective at boosting optical performance, these solutions can add mechanical complexity and control system requirements. Another approach is the use of multi-tube receivers, which can enhance heat collection and reduce stress on any single tube [19]. However, this can increase the receiver's thermal mass and potential heat loss area.

In contrast to these approaches, the present study investigates a different design philosophy: enhancing the thermal stability through a passive, geometric modification of the absorber tube itself, while retaining the simplicity of a single-tube evacuated receiver configuration. This proposed Concave-Wall Designs (CWD) are not intended to compete with adaptive optics on peak optical efficiency, but rather to offer a potentially more robust and mechanically simpler solution to the fundamental problem of non-uniform thermal loading. By strategically redesigning the absorber surface to passively bifurcate the concentrated flux, we aim to mitigate damaging hotspots at their source. The unique contribution of this work is therefore to systematically evaluate if this passive, geometric redesign can yield a crucial improvement in the conditions for thermal durability with only a negligible trade-off in optical performance, offering a distinct and complementary pathway for developing more reliable LFR systems.

These geometries replace portions of the conventional circular tube with inward-curving walls, effectively creating partial cavity structures. The idea is that these concave profiles can enhance optical performance by 1) increasing the effective acceptance angle, thereby capturing more reflected rays, especially during off-peak solar hours and low solar angles. 2) Promoting internal reflections within the concave structure, potentially increasing the probability of photon absorption. 3) Redistributing the incident solar flux over a larger or differently oriented surface area, potentially mitigating the extreme flux peaks and improving uniformity compared to the conventional design.

The main objective of this work is to conduct a detailed comparative analysis of the optical performance of the proposed CWD 45° and CWD 90° absorber geometries against the conventional ASB design within a representative LFR system configuration. The novelty of this study lies in the systematic optical assessment of these specific concave absorber shapes using detailed ray-tracing simulations, providing quantitative insights into optical efficiency, energy capture, and flux distribution characteristics under varied operational conditions. Specifically, this research aims to: 1) Model the ASB, CWD 45°, and CWD 90° absorber geometries integrated with secondary optics within a defined LFR system model (based on LFR1832 specifications). 2) Employ Monte Carlo ray-tracing simulations using Tonatiuh++ to accurately predict the optical behaviour of the system with each absorber design. 3) Quantify and compare the optical efficiency of the three designs across different geographical locations representing varying latitudes and under different seasonal conditions. 4) Analyze and compare the resulting heat flux distribution patterns on the absorber surfaces to understand the potential thermal loading characteristics associated with each design. 5) studying the effect of the interception ratio on optical efficiency for solar receivers of LFR system.

2. The proposed concave absorber and the reference receiver

2.1. The physical model of the concave receiver

The concave wall design (CWD) was introduced for the first time in this study as a new solution that aims to overcome the challenges found in previous receiver tubes, like decreasing the optical efficiency in winter and non-homogeneous thermal conditions on the surface tube. The CWD design features concave parabolic walls surrounding a metal tube, with air evacuated between the tube and the walls. It more effectively redirects solar radiation onto the absorber surface, enhancing absorption efficiency and improving heat-flux uniformity around the tube, thereby increasing the overall optical efficiency. The concave shape also helps to confine radiation and reduce scattering, which significantly reduces heat loss and increases system efficiency. The main objective of introducing CWD is to enhance efficiency and address the problems of irregularity caused by uneven distribution of solar heating as the sun travels across the sky.

The newly developed CWD 45° and CWD 90° designs are based on an evacuated tube design, featuring four concave walls that together form the absorber surface. The direction of slop of these walls determines the specific model. In CWD 45°, the concave walls are arranged so that their upper side edges form a 45-degree angle to the horizontal axis. And in CWD 90°, the concave walls were positioned at a 90-degree angle, Fig. 1 shows the CWD 45° Absorber Tube Model, CWD 90° Absorber Tube Model, and ASB Absorber Tube Model. The four surfaces of the CWD 45 are a, b, c, and d, while the surfaces of CWD 90 are TR (Top right), TL (Top left), DL

(Down right), and DR (Down left).

2.1.1. Geometric modeling for parabolic walls absorbed tube

The mathematical equation for the absorbing wall, which was used in this study and is expressed by the parabola equation in a two-dimensional system, is presented as follows [20]:

$$y^2 = 4P.x \tag{1}$$

where x and y are the two-dimensional coordinates of the parabola, and P is the parabolic focal length. Table 1 shows the design's parameters for the wall absorber in the new configuration CWD 45/90°.

The design parameters for the novel concave walls, presented in Table 1, were derived from a set of practical design constraints intended to create a geometrically significant cavity while maintaining compatibility with standard receiver dimensions. The Diameter (wp) of 50 mm and Depth (hp) of 10 mm were selected as the primary independent variables. These define a reasonably deep cavity capable of influencing the flux distribution, with an outer dimension that fits comfortably within a standard 70 mm OD absorber tube form factor. The Focal length (r_r) of 15.63 mm and Linear Diameter (L) of 55 mm are not arbitrary values; they are the direct mathematical results derived from the parabola equation (Eq. (1)) to ensure a smooth, continuous parabolic curve that spans the specified 50 mm diameter and 10 mm depth. This approach ensures a consistent and reproducible geometric definition for the analysis.

It is important to clarify that we maintained the same concentration ratio and, consequently, did not increase the tube circumference. Although increasing the tube diameter can enhance optical efficiency by capturing more reflected solar radiation, it also leads to greater thermal losses due to the increased surface area. The parameters in Table 1, including the focal length of 15.63 mm, were specifically derived to achieve a concave wall depth of 10 mm while maintaining a total circumference nearly identical to the 219 mm of the reference ASB receiver. This methodological choice ensures that our comparison isolates the effect of geometric shape from the effects of concentration ratio or surface area.

The rim angle (φr) is achieved by the following equation [21]:

$$\varphi r = \sin^{-1}\left(\frac{Wa}{rr}\right) \tag{2}$$

Where (Wa) is the width of the collector aperture is obtained via the following equation:

$$Wa = 4p.\tan\left(\frac{\varphi r}{2}\right) \tag{3}$$

(r_r) is the distance between the rim of the reflector and the focal center, which is called as the radius of rim:

$$r_r = \frac{2P}{1 + \cos(\varphi r)} \tag{4}$$

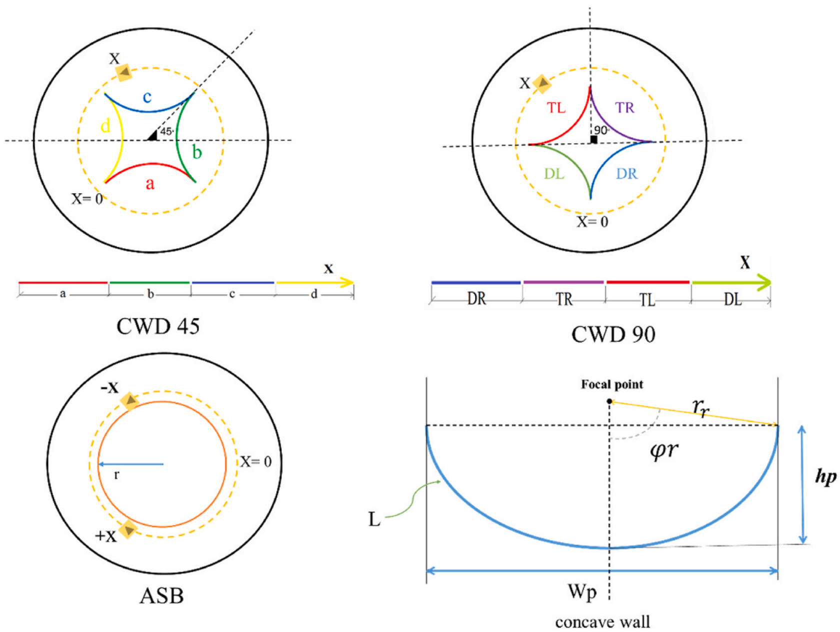

Fig. 1. CWD 45 Absorber Tube Model, CWD 90 Absorber Tube Model, ASB Absorber Tube Model, and shows the parameter for the concave absorb wall.

Table 1
The parameters for wall absorber.

Diameter	*wp*	50 mm
Depth	*hp*	10 mm
Focal length	r_r	15.63 mm
Linear Diameter	*L*	55 mm

The parabolic vertical height is calculated via the following equation:

$$hp = \frac{wa^2}{16p} \tag{5}$$

2.1.2. Defining the optical parameters

The aim of using the proposed geometry is to increase acceptability (CAP) by increasing the angle of half-acceptance θ or concentrated ratio *Cr*.

Where the acceptability (CAP) is given by this equation [20]:

$$CAP = Cr.\sin\theta \tag{6}$$

The proportion between the number of rays entering the system and the number of rays admitted, the CPC is referred to as the acceptability:

$$A = N_{abc} / N_{rec} \tag{7}$$

N_{abc}: number of rays hitting the absorber.

N_{rec}: number of rays entering the CPC.

However, the primary difference lies between the new designs for the evacuated tube CWD 45 and CWD 90 and the conventional one, ASB, in the geometrical profile of the absorbed surface and its relative positioning within the evacuated glass tube. All configurations maintain almost the same concentration ratio by preserving the same total circumference length for the surface of the absorber across all designs.

The CWD 45 absorber consists of four walls, each with a length of 55 mm, forming a closed surface around the absorber. The total circumference (C) of this model is given by the summation of the four surfaces a, b, c, and d, which would be equal to 220 mm.

Similarly, the CWD 90 model consists of four walls, and each wall measures 55 mm, so the total circumference remains 220 mm.

For the ASB reference design, the absorber tube has radius r, giving a circumference of 219 mm.

The geometric concentration ratio (Cr) is a fundamental parameter that governs the performance of a concentrating solar collector. It is defined as the ratio of the primary reflector's total aperture width (W) to the absorber's circumference (C). For the LFR system under study, the total reflector width (W) is constant at 5.76 m (18 mirrors × 0.32 m each). To ensure a fair and direct comparison, the novel CWD 45° and CWD 90° designs were intentionally engineered to have an absorber circumference (C) nearly identical to that of the conventional ASB model. By keeping both W and C constant, the concentration ratio (Cr ≈ 27) is maintained across all three designs. This methodological choice is critical, as it isolates the impact of the absorber's geometric shape. Any observed differences in

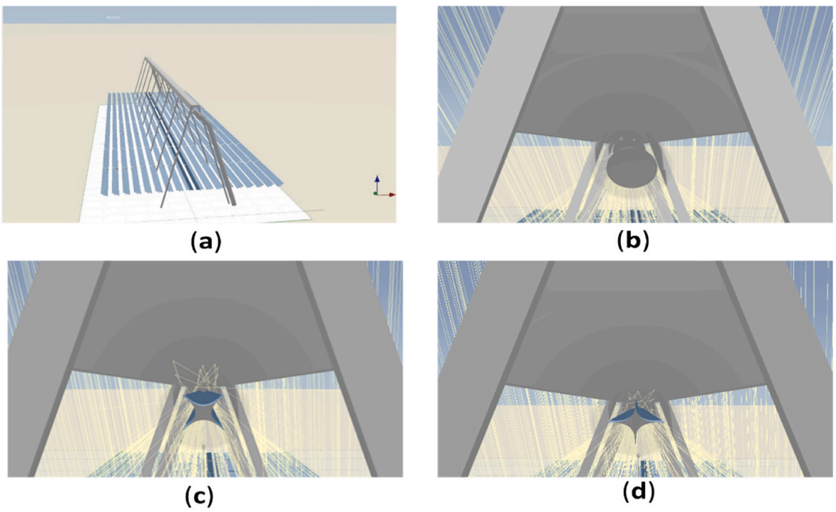

Fig. 2. (a) Tonatiuh++ model of the (a) overview of the IDEA LFR1832 collector. (b) CWD 45 receiver design (c) CWD 90° receiver design (d) ASB receiver model.

optical efficiency or heat flux distribution can therefore be attributed directly to the new geometries, rather than to a variation in the concentration level.

2.2. The LFR specifications and reference receiver

The LFR1832 linear Fresnel reflector (LFR) system, developed by IDEA SRL and installed at the Cyprus Institute, embodies the current industry-standard ASB receiver configuration. The system consists of 288 precisely curved cylindrical mirrors (each 2m × 0.32m) arranged in 18 rows with 0.2m inter-row spacing, creating a total collection area of 184.32 m^2 with a geometric concentration ratio of 27:1 as mentioned [17]. The solar concentration system directs incident radiation onto a 32-m-long high-performance absorber assembly consisting of an evacuated stainless-steel tube (70 mm OD/66 mm ID) enveloped by a borosilicate glass cover (115 mm OD) with exceptional transmittance ($\tau = 0.95$) and low emittance ($\varepsilon = 0.88$). The heat transfer fluid is mineral oil, which circulates in a thermally optimized south-north flow configuration, as shown in Fig. 2 (a); the entire system is modelled using Tonatiuh++ ray-tracing software to characterize optical performance, where Table 2 shows the technical specifications of LFR1832 system with the existing configuration receiver ASB.

It is important to emphasize that for this comparative study, the geometric concentration ratio was intentionally kept constant ($Cr \approx 27$) for all three designs. This was achieved by designing the CWD absorbers to have a wetted perimeter nearly identical to the circumference of the reference ASB absorber. This methodological choice is critical, as it isolates the impact of the absorber's geometric shape on optical efficiency and heat flux distribution, allowing for a direct and fair comparison. Any observed performance differences can therefore be attributed to the novel geometries themselves, rather than to variations in the concentration level.

2.3. Manufacturing considerations and feasibility

A critical aspect for the practical implementation of the novel CWD designs is their manufacturing feasibility. While more complex than conventional circular tubes, the proposed cross-sections are achievable with established industrial metal forming technologies. Tube hydroforming, in particular, stands out as a highly suitable method. This process involves placing a standard circular tube into a die cavity shaped to the desired CWD profile and then using internal high-pressure fluid to expand the tube, forcing it to conform to the die's shape. This technique is widely used in the automotive and aerospace industries to produce strong, precise, and seamless components from materials such as stainless steel.

Alternative methods could include extrusion for more ductile materials or roll forming followed by seam welding. While the manufacturing cost of a CWD tube would likely be higher than that of a standard circular tube, these established processes confirm the technical feasibility of the design. A full techno-economic analysis would be required to evaluate whether the significant gains in thermal uniformity and predicted durability offset the additional manufacturing complexity and cost, but the design is not considered to be constrained by fundamental manufacturing limitations.

3. Optical analysis

This section outlines the comprehensive optical analysis performed to evaluate the novel receiver designs. It details the simulation methodology, the software and parameters used, the specific scenarios investigated, and the key performance metrics employed for comparison.

Table 2
Technical Specifications of reference system LFR1832 [17].

Component	Parameter	Specification	Performance Value
Primary Reflector	Number of rows	18	–
	Individual mirror length	2 m	–
	Mirror width	0.32 m	–
	Inter-row spacing	0.2 m	–
	Reflectance (ρ_1)	–	0.924
Absorber tube	Tube material	stainless steel	–
	Outer diameter	70 mm	–
	Inner diameter	66 mm	–
	Absorptance (α)	–	0.92
Glass Cover tube	Material	Borosilicate glass	–
	Outer diameter	115 mm	–
	Inter diameter	109 mm	
	Transmittance (τ)	–	0.95
	Emittance (ε)	–	0.88
Secondary Reflector	Design type	Compound Parabolic Concentrator (CPC)	–
	Material	Silver-coated aluminium	–
	Reflectance (ρ_2)	–	0.883
	Acceptance angle	±29.9°	–
System Performance	Total aperture area	184.32 m^2	–
	Concentration ratio	27:1	–

3.1. Simulation methodology

The following subsections describe the systematic approach used to model and simulate the Linear Fresnel system. This methodology was designed to ensure high accuracy, reliability, and a fair comparison between the different absorber geometries under a wide range of operating conditions.

3.1.1. Tonatiuh++ model

This work implements the advanced open-source optical simulation tool Tonatiuh++ to conduct the detailed optical analysis for the proposed receivers. Tonatiuh++ operates as an open-source program for Monte Carlo ray tracing-based solar concentrator optical behaviour. As an essential tool in the solar energy sector, Tonatiuh++ assists researchers and designers through the modelling of reflective and refractive solar concentrator systems [22,23]. Through the Monte Carlo Ray Tracing (MCRT) method Tonatiuh++ simulates sunlight interactions with complex concentrator geometries, including Linear Fresnel systems [24]. Through this process, the software generates highly accurate predictions about optical performance by simulating light paths that include reflection and refraction along with absorption [25]. The C++ programming language combined with multi-threading support enables Tonatiuh++ to run simulations efficiently and fast for both small, large, and complex models [26]. Using this versatile tool, users can model a wide range of solar concentrator types and configurations, including heliostat fields and advanced dual-receiver systems, while also defining custom geometries and material properties for specific studies [27]. The optical predictions from Tonatiuh++ demonstrate more than 95 % accuracy when validated through experimental results The design optimization process benefits from this tool through its ability to enhance system efficiency by improving collector geometry and receiver placement and system layout for specific operational requirements [28]. The simulation accuracy of Tonatiuh++ when estimating total power and irradiance matches Sol Trace and TracePro yet small discrepancies exist in peak flux predictions [29]. Tonatiuh++ tool delivers precise optical models for LFC systems while optimizing geometric parameters through design optimization and validates results with experimental data and evaluates loss mechanisms, and provides non-imaging optics and solar tracking capabilities, and maintains cost-effectiveness and maintenance requirements analysis, which makes it a comprehensive platform for both research and real-world application development in this field [24].

3.1.2. Ray tracing methodology and numerical convergence

The advanced open-source Monte Carlo ray-tracing software Tonatiuh++, based on C++ operates as the main computational tool for this research through its validated framework from Tonatiuh [23,30]. The ray-tracing simulations use 10^7 rays as an optimized number to achieve high accuracy while maintaining computational efficiency. The error analysis performed by Montenon et al. [17], shows that using more than 10^7 rays produces relative errors in optical efficiency calculations below 0.1 %. The investigated facility contains 288 mirrors, which receive approximately 35,000 rays per mirror at the chosen ray count to produce statistically reliable results. The approach followed by using 5000 rays per mirror (totalling 1.44×10^6 rays for the entire system) but achieves better precision through increased sampling density. The reference benchmark of 10^9 rays was used to validate convergence, confirming that the selected 10^7 rays provide an optimal balance between computational tractability and simulation fidelity. The reliability of this methodology for optical efficiency analysis in concentrated solar power systems is supported by previous Tonatiuh++ simulations of Linear Fresnel Reflectors (LFRs) [30]. The following table, Table 3, shows all the parameters that have been used in this study.

3.1.3. Simulation scenarios

To ensure the credibility of the findings, the study was designed in two phases: model validation followed by a comprehensive performance analysis across diverse scenarios.

The computational framework was first validated against established experimental data to ensure its accuracy. This validation process, which is described in detail in Refs. [17,30,31], involved modeling the LFR1832 system located at the Cyprus Institute in Nicosia (35.14°N, 33.38°E). The simulations demonstrated excellent agreement with the reference performance data from the physical installation, confirming the fidelity of the model's geometry, optical properties, and overall setup for the subsequent analysis.

Following successful validation, the investigation was expanded to evaluate the optical performance of the ASB, CWD 45°, and CWD 90° absorber designs under a range of operating conditions. The scenarios were carefully selected to test the designs' adaptability to different environments and solar geometries.

Three cities were chosen to represent distinct climate zones and, crucially, to provide a wide range of solar elevation angles due to

Table 3
Ray-tracing simulation parameters for LFR optical analysis.

Parameter	Value/Description
Software	Tonatiuh++ (Monte Carlo raytracing, C++ based)
Ray count range n	1000 to 10^9 rays
Reference ray count N	10^9 rays
Error threshold beyond 10^7 rays	Below 0.1 %
Mirrors in facility	288 mirrors
Rays per mirror (at 10^7)	~35,000 rays per mirror
Rays per facility	5000 rays
Standard ray count used in study	10^7 rays

their different latitudes:

- Khartoum, Sudan (15.56°N): Representing a hot, arid climate with high solar elevation angles year-round.
- Nicosia, Cyprus (35.14°N): Representing a mid-latitude Mediterranean climate with moderate and highly seasonal solar elevation angles.
- Miskolc, Hungary (48.3°N): Representing a high-latitude temperate continental climate, characterized by low winter solar elevation angles, which presents a significant challenge for LFR systems.

To analyze performance at the extremes of the solar calendar, simulations were conducted at each location for: Summer Solstice (June 21) to evaluate performance when the sun is at its highest path in the sky, resulting in maximum daily solar elevation. Winter Solstice (December 21): to evaluate performance when the sun is at its lowest path, resulting in minimum daily solar elevation and challenging incidence angles.

For all simulations, a constant Direct Normal Irradiance (DNI) of 900 W/m^2 was used from sunrise to sunset. This standard practice isolates the impact of the collector and receiver geometry from the variable effects of atmospheric conditions, allowing for a direct and fair comparison of the optical performance of the three designs.

3.2. Performance metrics definition

To enable a fair and comprehensive comparison of the receiver designs, we defined a set of key performance metrics. These quantify both the total energy collected and the quality and uniformity of its delivery, which are critical for long-term system reliability.

3.2.1. Optical efficiency

The primary metric for evaluating the performance of the solar collector designs in this study is optical efficiency η_{opt}. It is defined as the ratio of the solar energy absorbed by the receiver tube (*Qabc*) to the total direct solar energy incident on the collector's aperture area (*Qin*) [32,33].

$$\eta_{\ opt} = Qabc / Qin \tag{8}$$

The optical efficiency is not a constant value; it is highly dependent on the sun's position relative to the collector. This angular dependence is quantified by the Incidence Angle Modifier (IAM), a factor that accounts for performance losses at off-normal solar angles. For a Linear Fresnel Collector, the IAM is a function of the transverse (θ_{-T}) and longitudinal (θ_{-L}) incidence angles.

The overall optical efficiency at any given time can therefore be expressed as the product of the peak optical efficiency ($\eta_{opt,max}$) and the IAM [34,35]:

$$\eta_{opt(\theta L,\theta T)} = KL(\theta L).KT(\theta T).\eta_{opt,max} \tag{9}$$

where $\eta_{opt,max}$ is the maximum possible efficiency, achieved at normal incidence ($\theta_{-L} = 0$, $\theta_{-T} = 0$) when the IAM is equal to 1. The ray-tracing simulations conducted in this work inherently calculate the absorbed energy (*Qabc*) for varying sun positions throughout the day, thus providing a precise measure of the collector's optical efficiency under real-world operational angles.

3.2.2. Flux distribution and thermal uniformity

Beyond high optical efficiency, the long-term viability and reliability of a solar receiver depend critically on its ability to manage thermal loads. Therefore, a second key performance metric in this study is the uniformity of the solar heat flux distribution on the absorber surface.

A highly non-uniform flux distribution, characterized by intense peaks or "hotspots," can induce severe thermal stresses within the absorber material and its selective coating. These stresses lead to material fatigue, cracking, and premature system failure, ultimately compromising the operational lifespan and increasing maintenance costs. Consequently, a design that promotes a more uniform heat flux is inherently superior to thermal management and structural stability perspective.

To quantitatively assess the uniformity of the heat flux, the standard deviation ($S_{q''}$) of the radiant flux across the absorber's perimeter is employed as a key statistical metric. It is calculated using the following equation [31]

$$S_{q''} = \sqrt{\frac{\sum_{i=1}^{Nf} \left(q_i'' - q''\right)^2}{N_f}} \tag{10}$$

Where:

$S_{q''}$ is the standard deviation of the heat flux [W/m^2].

q_i'' is the radiative flux on an individual surface element *i* of the receiver mesh [W/m^2].

$\overline{q}''$ is the mean radiative flux, calculated as the average of all q_i'' values across the entire absorber surface [W/m^2].

N_f is the total number of discrete surface elements (mesh faces) representing the receiver's geometry.

A lower standard deviation signifies a more uniform heat flux distribution, indicating lower thermal gradients and reduced mechanical stress. Conversely, a higher standard deviation points to significant non-uniformity and the presence of potentially damaging hotspots. By calculating this value for each design under various operating conditions, this study provides a direct and robust comparison of their ability to achieve effective thermal management.

3.2.3. Ray tracing and interception analysis

While the overall optical efficiency (η_{opt}) provides a single, comprehensive performance value, it is instructive to deconstruct it into its constituent factors to better understand the sources of optical losses. The total efficiency is a product of material properties and the system's geometric efficiency. This can be expressed [36]:

$$\eta_{opt} = \alpha.\rho.\tau.IC \tag{11}$$

Where:

ρ (rho) is the reflectivity of the primary mirror surfaces.

τ (tau) is the transmittance of the glass envelope surrounding the absorber.

α (alpha) is the absorptance of the selective coating on the receiver tube surface.

IC is the Interception Factor.

The first three terms (ρ, τ, α) are material properties that are assumed to be constant in this study. The Interception Factor (IC), however, is a purely geometric efficiency metric. It is not a material property but rather a measure of how effectively the receiver's geometry (including the secondary concentrator) captures the concentrated sunlight reflected from the primary mirrors.

It is defined as the ratio of the number of rays that successfully strike the absorb tube to the number of rays that enter the secondary optic assembly [37]:

$$IC = K' / K'' \tag{12}$$

K': Number of rays striking the absorb surface.

K'': Number of rays entering the secondary optics.

The Interception Factor is a critical performance metric for this study because it directly quantifies the impact of the new CWD 45° and CWD 90° geometries. A value of IC < 1 indicates that some rays are lost due to "spillage" they miss the absorber tube after passing through the secondary optic. By analyzing the IC for each design under different solar conditions, we can isolate and evaluate the geometric advantages or trade-offs of each shape in capturing the available solar radiation.

4. Results and discussions

This section presents the results of the optical simulations for the three absorber designs (ASB, CWD 45°, and CWD 90°). The performance is evaluated based on the key metrics of optical efficiency and heat flux distribution uniformity, as defined in the previous section. The analysis covers all simulated geographical locations and seasonal conditions to provide a comprehensive comparison.

4.1. Optical efficiency analysis

This section analyses the optical efficiency of the three absorber designs. The daily performance curves for summer and winter

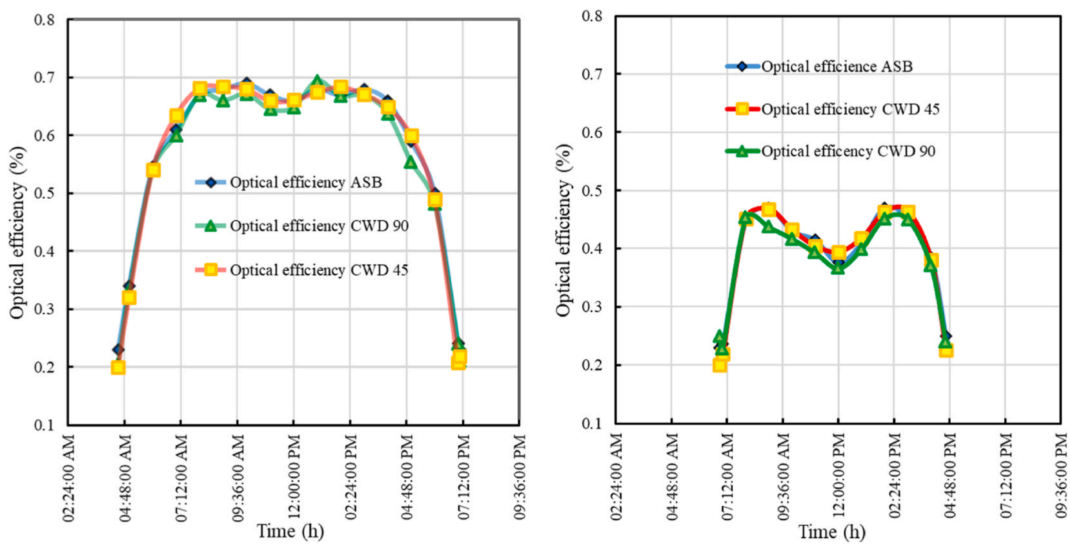

Fig. 3. Optical efficiency of the LFR system in Nicosia for the ASB, CWD 45, and CWD 90 models on (a) June 20, (winter solstice) and (b) December 21, (winter solstice).

solstices in Khartoum, Nicosia, and Miskolc are presented in Figs. 3–5. To facilitate a direct comparison, the key performance values, specifically the peak midday efficiency, are summarized in Table 4.

A primary trend observed across all locations is the significant seasonal variation in performance, with summer solstice efficiencies being substantially higher than those during the winter. This is an expected outcome for LFR systems, driven by the lower solar elevation angles and consequently greater cosine losses during winter months.

While peak midday efficiency provides a valuable snapshot of performance, the total daily energy yield, a metric that integrates performance from sunrise to sunset, offers a more holistic and practical comparison. Table 5 presents this integrated energy yield for all simulated scenarios. The results provide quantitative support for the trends observed in the daily efficiency curves. In high-insolation environments like Khartoum, where the sun is high for most of the day, the daily energy yields are nearly identical across all three designs.

However, in mid- and high-latitude locations, the integrated metric clearly quantifies the advantages of the novel geometries. In the challenging winter conditions of Nicosia, the CWD 45° design captures 2.22 kWh/m^2/day, a meaningful 5.7 % increase in daily energy compared to the 2.10 kWh/m^2/day of the conventional ASB. Similarly, in Miskolc's winter, both CWD designs outperform the ASB, with the CWD 90° capturing 1.91 kWh/m^2/day (a 3.2 % increase), validating its superior performance at the extremely low sun angles experienced at sunrise and sunset. Crucially, this analysis also reinforces the primary value proposition of the CWD 90° design: its substantial improvements in thermal flux uniformity are achieved with a negligible impact on energy capture, with its daily yield consistently remaining within 1–2 % of the ASB under most conditions.

4.1.1. Performance in high-insolation and mid-latitude environments (Khartoum & nicosia)

In Khartoum, which benefits from high solar elevation angles year-round, all three designs demonstrated excellent and nearly identical optical performance. As shown in Fig. 5 and Table 5, the performance curves are tightly clustered, with negligible differences between the models. This indicates that when the sun is predominantly high in the sky, the simple circular geometry of the ASB is sufficient for maximum energy capture, and the more complex CWD geometries offer no distinct optical advantage.

In the mid-latitude climate of Nicosia, a more sophisticated picture emerges. While all designs achieved comparable peak efficiencies around 0.69 % during the summer solstice, their performance diverges at lower solar elevations. A key distinction emerges during the shoulder hours of the operational day. In Nicosia during the summer solstice, for example, during the early morning (07:00–09:00) and late afternoon (15:00–17:00) operational periods, the CWD 45° design shows an average optical efficiency that is 3–5 % higher than the conventional ASB, as shown in Fig. 3. A similar, even more pronounced advantage is observed during the winter. While this gain may appear small on the daily efficiency graph, it is consistent and contributes directly to a higher total daily energy yield, as shown in Table 5. It is essential to note that while the simulations span from sunrise to sunset for completeness, a typical LFR plant typically operates only when DNI levels are sufficient (e.g., >200 W/m^2), making performance during these mid-morning and mid-afternoon hours particularly relevant to overall energy production.

The 45-degree angled walls, in the CWD 45° design, appear to provide an optimal compromise, creating a wider effective aperture for capturing oblique rays from the side mirrors without significantly shadowing itself during midday. The CWD 90° design, conversely, sometimes showed a slight dip in performance compared to the other two during these shoulder hours. This can be attributed to its vertical walls, which may cause some self-shading or block incoming rays at very low transverse angles, a trade-off for its primary function of homogenizing flux, which is discussed later.

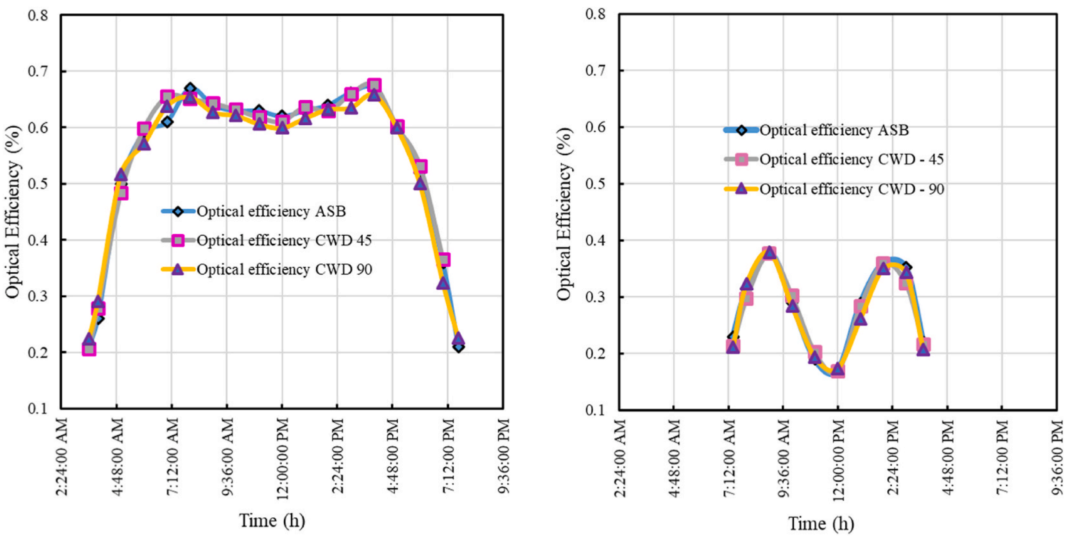

Fig. 4. Optical efficiency of the LFR system in Miskolc for the ASB, CWD 45, and CWD 90 models on (a) June 20, (summer solstice) and (b) December 21, (winter solstice).

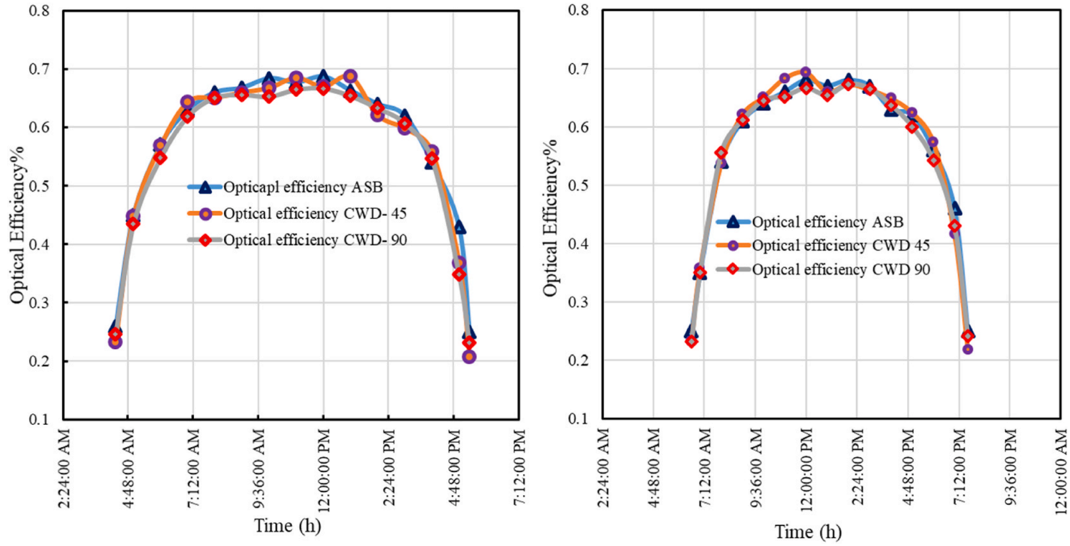

Fig. 5. Optical efficiency of the LFR system in Khartoum for the ASB, CWD 45°, and CWD 90° models on (a) June 20, (winter solstice) and (b) December 21, (winter solstice).

Table 4
Summary of peak midday optical efficiencies ($\eta_{opt,peak}$) for each design.

Location	Season	ASB	CWD 45°	CWD 90°
Khartoum (15.56°N)	Summer Solstice	0.687	0.67	0.667
	Winter Solstice	0.68	0.693	0.666
Nicosia (35.14°N)	Summer Solstice	0.66	0.661	0.648
	Winter Solstice	0.376	0.394	0.366
Miskolc (48.3°N)	Summer Solstice	0.62	0.611	0.599
	Winter Solstice	0.38	0.377	0.379

Table 5
Comparison of peak midday optical efficiency and total daily absorbed solar energy.

Location	Season	Design	Peak Optical Efficiency ($\eta_{opt,peak}$)	Daily Energy Yield (kWh/m^2/day)
Khartoum (15.56°N)	Summer Solstice	ASB	0.687	5.10
		CWD 45°	0.670	5.08
		CWD 90°	0.667	5.05
	Winter Solstice	ASB	0.680	4.15
		CWD 45°	0.693	**4.20**
		CWD 90°	0.666	4.08
Nicosia (35.14°N)	Summer Solstice	ASB	0.660	4.80
		CWD 45°	0.661	**4.85**
		CWD 90°	0.648	4.76
	Winter Solstice	ASB	0.376	2.10
		CWD 45°	0.394	**2.22**
		CWD 90°	0.366	2.05
Miskolc (48.3°N)	Summer Solstice	ASB	0.620	4.55
		CWD 45°	0.611	**4.58**
		CWD 90°	0.599	4.52
	Winter Solstice	ASB	0.380	1.85
		CWD 45°	0.377	1.90
		CWD 90°	0.379	**1.91**

4.1.2. Performance in high-latitude environments (Miskolc)

The challenging, low-angle solar conditions of Miskolc most clearly highlight the adaptive benefits of the CWD geometries. Here, the ability to capture highly oblique rays is important, especially in winter. Both the CWD 45° and CWD 90° models showed a clear, although small, performance advantage over the ASB reference, particularly during the winter solstice (Fig. 4). They consistently delivered 1–4 % higher efficiency throughout the day. The CWD 90° design was particularly effective at sunrise and sunset, demonstrating that its vertical cavity-like structure is adept at trapping rays at extremely low angles, which would otherwise miss the conventional circular ASB tube. The CWD 45° design proved to be the most balanced performer, maintaining a consistent edge over the ASB without the slight midday performance dip sometimes seen in the CWD 90° model.

In summary, the optical efficiency analysis reveals a clear, location-dependent trend that distinguishes the three designs. While the ASB is optically sufficient in high-sun environments like Khartoum, its limitations become apparent as solar angles decrease. The CWD 45° design emerges as the superior choice for maximizing daily energy yield, especially in mid-to-high latitudes, due to its enhanced ability to capture oblique radiation during morning and evening hours. The CWD 90° design also shows advantages over the ASB in low-light conditions, although its geometry suggests its primary benefit may not be in maximizing total energy capture, but rather in how that energy is distributed.

It is essential to contextualize these optical efficiency findings within the primary objective of this study. While the CWD 45° design demonstrates a modest potential to increase daily energy yield in some scenarios, the CWD 90° design does not aim to outperform the ASB in raw energy capture. Instead, these results should be viewed as a successful validation of a critical design trade-off. The findings confirm that the CWD 90° geometry can achieve its primary goal, an improvement in heat flux uniformity, as will be shown in the following section, while remaining optically competitive and incurring a negligible penalty in daily energy capture. The following section, therefore, moves from how much energy is captured to how that energy is distributed across the absorber surface, which is the key determinant of thermomechanical stability for LFR receivers.

4.2. Heat flux distribution and thermal stability analysis

While optical efficiency dictates the total energy captured, the uniformity of the solar heat flux distribution governs the receiver's long-term structural integrity and reliability. This section provides a detailed analysis of the flux patterns on the three absorber designs, linking their geometric features and the seasonal variations in solar angle to the resulting thermal loads. The visual flux distributions for representative summer and winter cases are presented in Figs. 6–11, and a quantitative comparison using the standard deviation of the flux is summarized in Table 6.

4.2.1. Qualitative flux pattern analysis

The flux maps reveal fundamentally different thermal loading patterns that are a direct consequence of both the receiver's geometry and the sun's elevation angle. In summer, at high solar elevations, the concentrated flux is especially intense and strongly focused on the receiver. For the ASB, this creates the classic, narrow "crescent moon" hotspot on its bottom surface. The CWD 45° similarly concentrates this energy on its lower surface 'a', in some cases creating an even sharper, more intense hotspot due to it focusing geometry. (Figs. 6–8).

Even with high-angle summer sun, the CWD 90°'s vertical cavity design successfully bifurcates (splits) the flux into two more diffuse regions on its lower surfaces (DR and DL). This prevents the formation of a single, damaging peak, immediately demonstrating its superior thermal management.

figures (1S,2S,3S) in the Appendix represent the flux distribution for the three designs (CWD 45°, CWD 90°, and ASB) at 12:00 noon

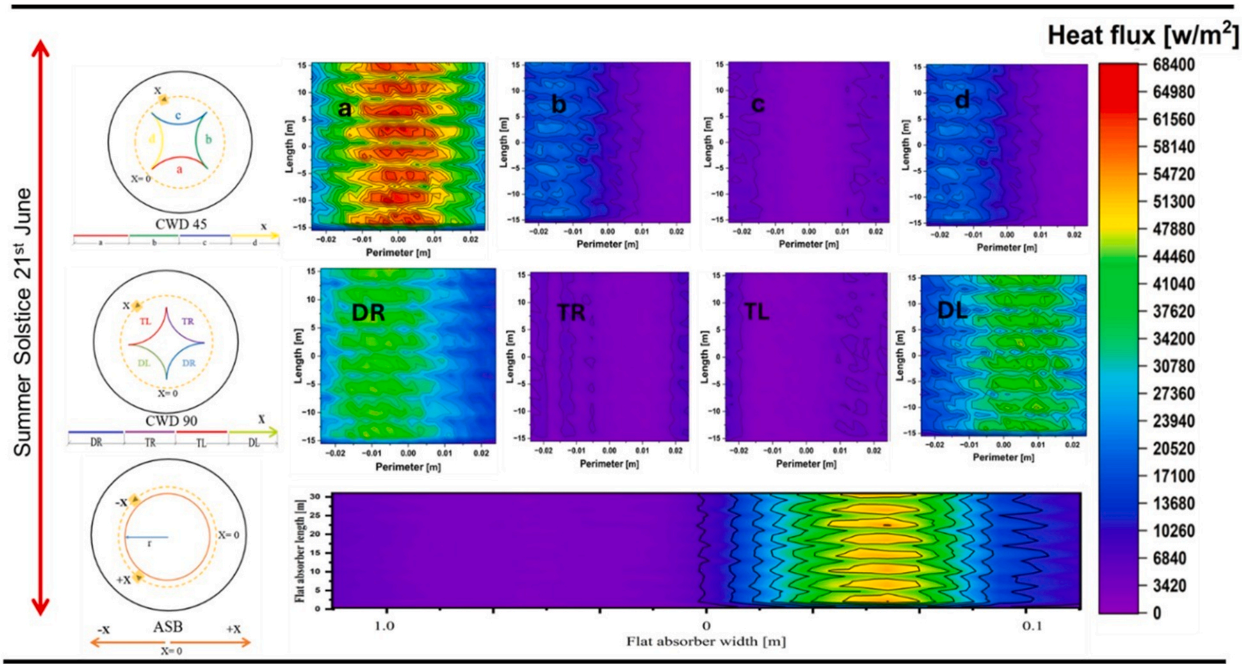

Fig. 6. Flux distribution for the three designs (CWD 45°, CWD 90°, and ASB) at 12:00 p.m. in Nicosia during the summer solstice.

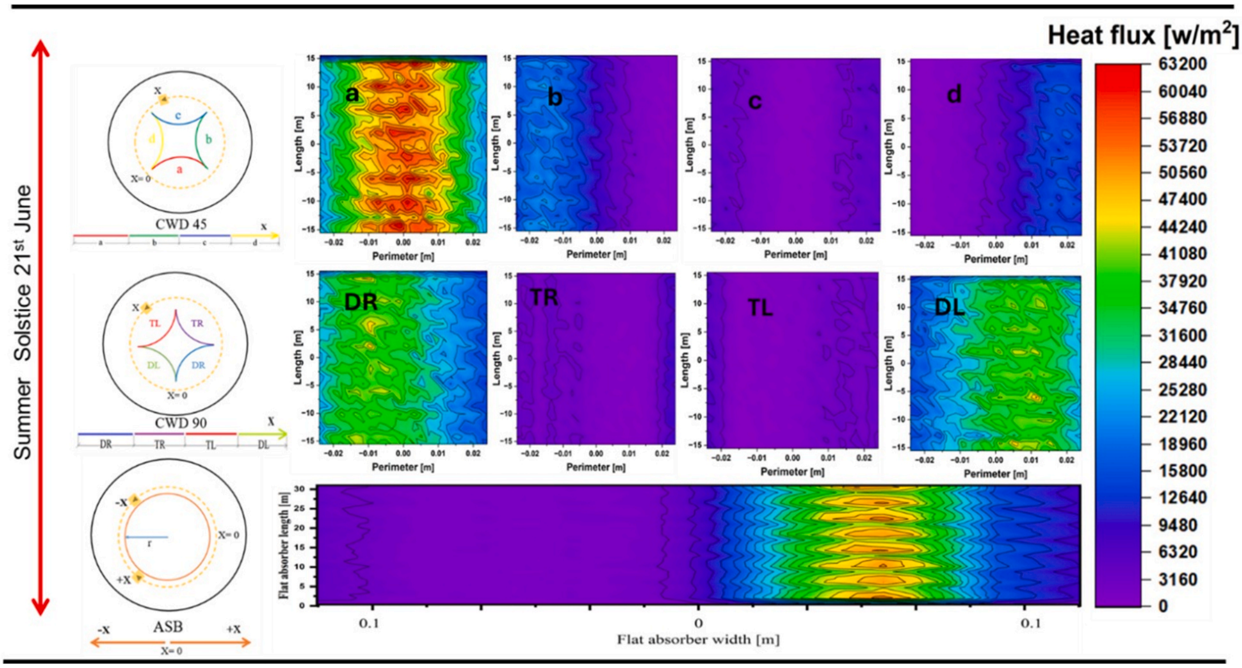

Fig. 7. Flux distribution for the three designs (CWD 45°, CWD 90°, and ASB) at 12:00 p.m. in Khartoum during the summer solstice.

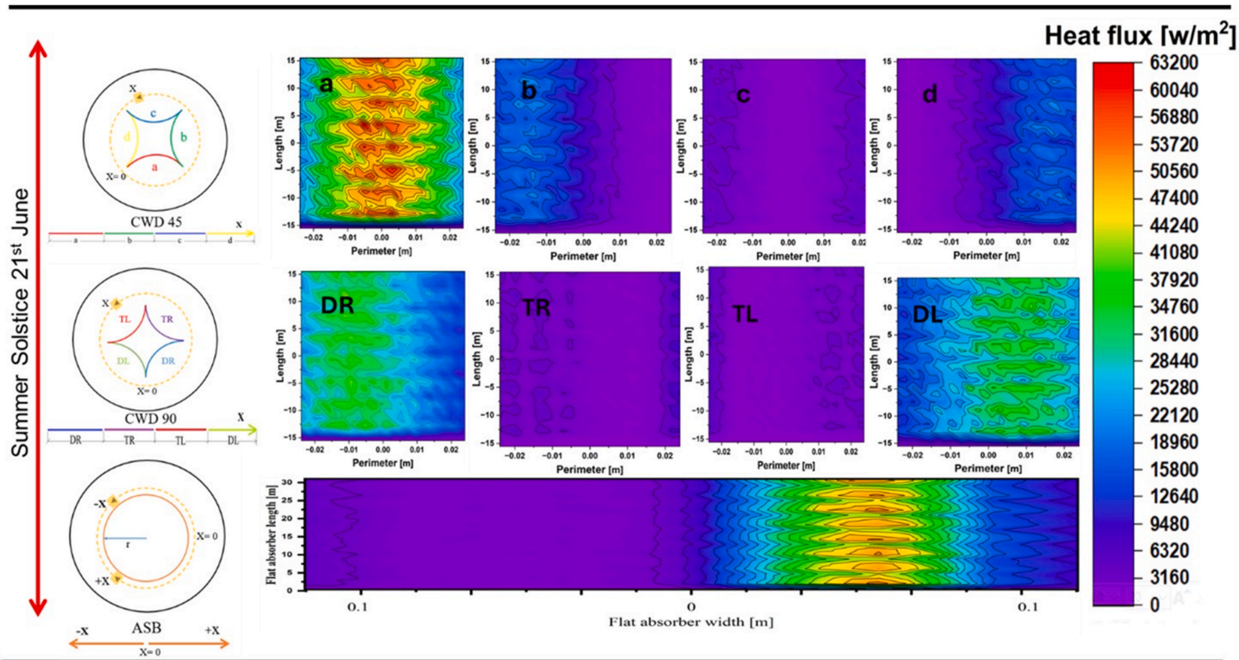

Fig. 8. Flux distribution for the three designs (CWD 45°, CWD 90°, and ASB) at 12:00 p.m. in Miskolc during the summer solstice.

in Nicosia, Khartoum, and Miskolc during the winter solstice. These appendix figures (1S, 2S, 3S) visually confirm that even under the diffuse, low-angle sun of winter, the ASB and CWD 45° designs continue to produce a single, concentrated hotspot, whereas the CWD 90° successfully maintains its bifurcated and more uniform flux pattern.

The seasonal change is most dramatic for the ASB and CWD 45°. With lower sun angles, the focal point becomes less sharp, and the total energy is lower, but the fundamental problem of a single, dominant hotspot persists, even so at a lower intensity. The CWD 90° continues to excel. Its ability to split the beam remains effective, resulting in a balanced distribution even under low-angle winter

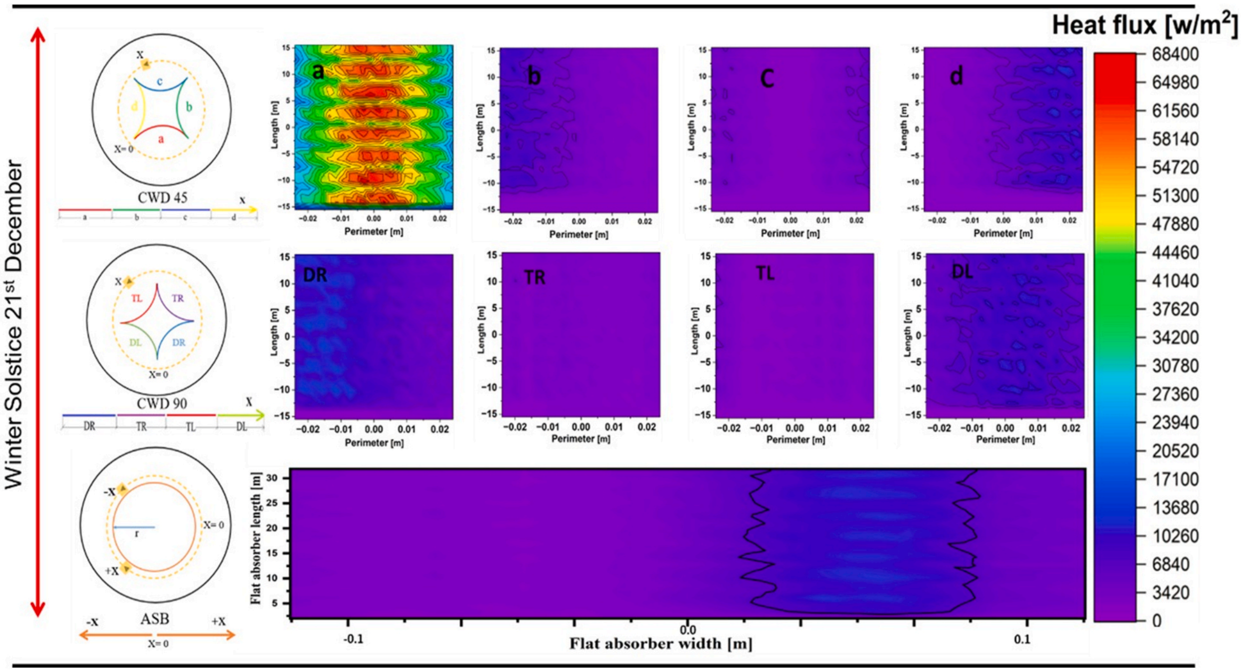

Fig. 9. Flux distribution for three designs (CWD 45°, CWD 90° and ASB) at 8 a.m. for Nicosia city during the winter solstices.

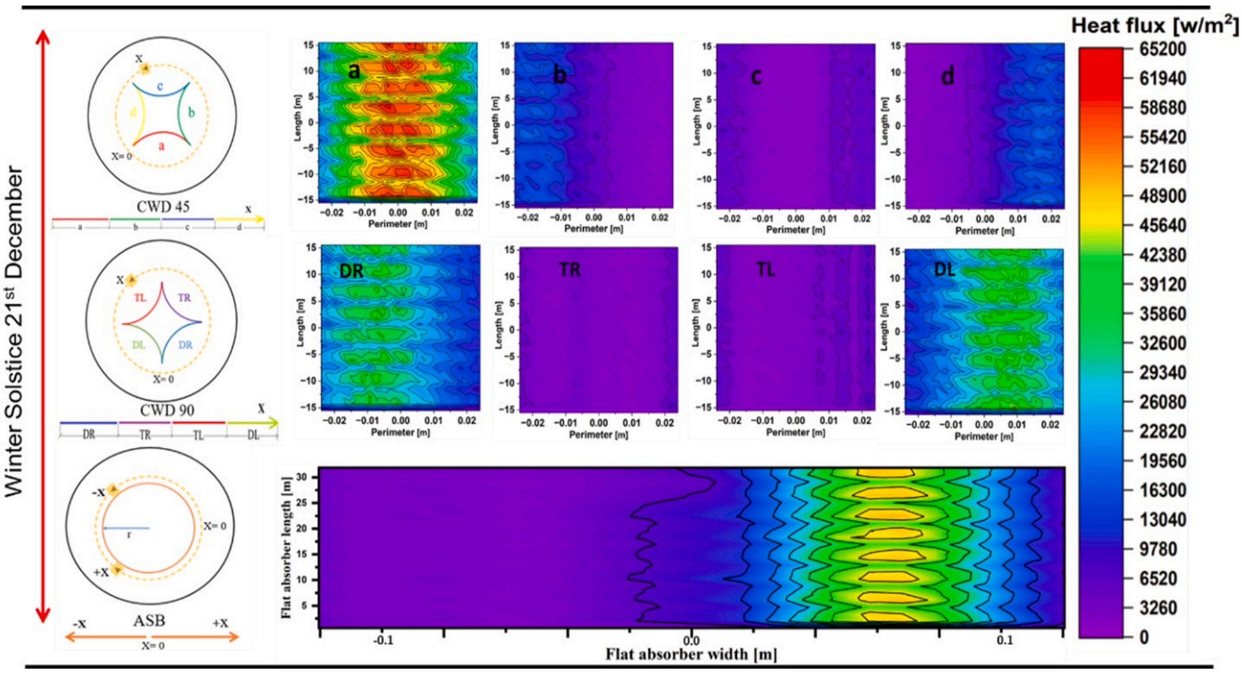

Fig. 10. Flux distribution for three designs (CWD 45°, CWD 90° and ASB) for Khartoum city during the 8 a.m. winter solstice.

conditions. This adaptability is a key advantage, ensuring more consistent thermal loading across different seasons (Figs. 9–11).

The ASB receiver demonstrates the classic, highly problematic flux profile of LFR systems. Its convex lower surface acts as a single focal point for the incoming rays, creating an intense, narrow hotspot. This leads to a peak-to-average flux ratio that is extremely high, causing severe temperature gradients between the irradiated bottom and the shaded top. This is the root cause of the circumferential thermal stresses that plague conventional absorbers.

figures (4S,5S,6S) in the Appendix represent the flow distribution for the three designs (CWD 45°, CWD 90°, and ASB) at 8:00 a.m.

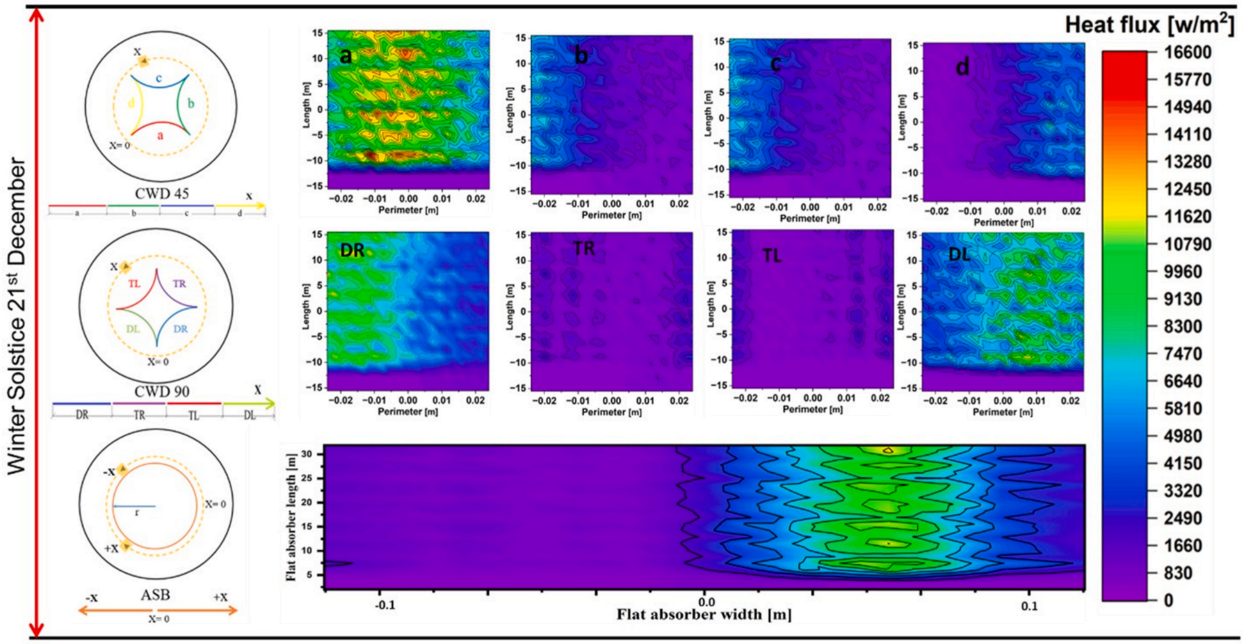

Fig. 11. Flux distribution for three designs (CWD 45°, CWD 90° and ASB) for Miskolc city during the 8 a.m. at winter solstice.

in Nicosia, Khartoum, and Miskolc during the summer solstice. As shown in the Appendix (Figs. 4S, 5S and 6S), these low-sun-angle morning conditions produce a highly skewed and asymmetric flux on the ASB and CWD 45° receivers, while the CWD 90° geometry demonstrates a remarkable ability to intercept and redistribute this skewed radiation into two more balanced focal regions.

The CWD 45° geometry represents an intermediate case. The concave bottom surface (surface 'a') still concentrates the flux intensely, similar to the ASB. In fact, its shape can even lead to a slightly higher peak flux, as it more effectively focuses the central rays. However, its 45-degree angled side walls (surfaces 'b' and 'd') begin to intercept rays from the outer primary mirrors, slightly broadening the overall irradiated zone. This design essentially trades a single, very sharp hotspot for a slightly wider but still highly intense one, offering minimal improvement in thermal management, as the quantitative analysis will confirm.

The CWD 90° design fundamentally alters the flux pattern. The vertical walls (forming a rectangular-like cavity) prevent the formation of a single focal point. Instead, the incoming radiation is bifurcated, creating two distinct and significantly less intense focal regions on the lower surfaces (DR and DL). This geometric "splitting" of the concentrated beam is the key innovation. The result, clearly visible in the flux maps, is the near-total elimination of the red hotspots characteristic of the other two designs. The thermal load is more evenly distributed, which is the ideal characteristic for thermal stability.

4.2.2. Quantitative flux uniformity analysis

The visual evidence of improved flux distribution is strongly corroborated by the quantitative analysis presented in Table 6. This table now explicitly lists the mean absorbed heat flux and the standard deviation of the flux ($S_{q''}$), which serves as a direct measure for thermal non-uniformity. Across all simulated conditions, the data shows that while the mean absorbed flux delivered to each design is comparable (reflecting their similar optical efficiencies), the CWD 90° design unequivocally achieves the lowest standard deviation, confirming its superior thermal management capabilities.

The magnitude of this improvement is most pronounced under conditions of high solar flux when the risk of thermal damage is greatest. For instance, during summer midday in both Khartoum and Nicosia, the CWD 90° reduces the $S_{q''}$ by a significant ~10–11 % compared to the ASB. This is a direct quantitative measure of its ability to mitigate the intensity of the primary hotspot. The data in Table 6 also reveals a fascinating interaction between solar angle and flux uniformity. The most dramatic improvement is observed at low sun angles, particularly during the summer morning (8 a.m.), where the CWD 90° design shows a remarkable ~15 % reduction in $S_{q''}$ compared to the ASB in all scenarios. This is not an anomaly but a direct consequence of how the CWD 90° geometry manages the asymmetric radiation from the mirror field. At these low solar elevations, the incoming radiation is highly skewed, with mirrors on one side of the field contributing far more energy than the other. The single-focus geometries of the ASB and CWD 45° are unable to manage this asymmetry, resulting in a single, intense, and off-center hotspot, leading to a very high standard deviation. The CWD 90°, however, acts as a passive homogenizer. Its vertical cavity walls intercept the skewed flux and bifurcate (split) it between the two lower surfaces. This geometric "scrambling" of the asymmetric input prevents the energy from one side of the mirror field from overwhelming one spot on the receiver. This unique capability to manage skewed, off-peak flux is the primary reason for its exceptional performance under these challenging conditions.

The analysis reinforces a critical finding regarding the CWD 45° design. In nearly every scenario, it exhibits the highest standard

Table 6
Standard Deviation of Heat Flux ($S_{q''}$), Mean absorber flux, and Uniformity improvement for Representative Summer and Winter Time Slots.

Location	Season	Time	Design	Mean Absorbed Flux (kW/m^2)	Standard Deviation ($S_{q''}$) (kW/m^2)	Improvement in Uniformity (ASB vs. CWD 90°)
Khartoum (15.56°N)	Summer	8 a.m.	ASB	15.1	15.7	~15.3 %
			CWD 45°	15.0	17.4	
			CWD 90°	14.8	**13.3**	
	Summer	12 p.m.	ASB	16.7	16.5	~10.3 %
			CWD 45°	16.3	16.8	
			CWD 90°	16.2	**14.8**	
	Winter	8 a.m.	ASB	15.8	15.4	~14.3 %
			CWD 45°	16.1	17.3	
			CWD 90°	15.4	**13.2**	
	Winter	12 p.m.	ASB	16.5	16.4	~23.2 %
			CWD 45°	16.8	18.2	
			CWD 90°	16.2	**12.6**	
Nicosia (35.14°N)	Summer	8 a.m.	ASB	14.6	16.0	~13.8 %
			CWD 45°	14.8	18.0	
			CWD 90°	14.3	**13.8**	
	Summer	12 p.m.	ASB	16.0	16.5	~10.9 %
			CWD 45°	16.1	18.2	
			CWD 90°	15.7	**14.7**	
	Winter	8 a.m.	ASB	6.8	4.0	~2.5 %
			CWD 45°	7.1	19.1	
			CWD 90°	6.6	**3.9**	
	Winter	12 p.m.	ASB	9.1	5.6	~5.4 %
			CWD 45°	9.6	19.2	
			CWD 90°	8.9	**5.3**	
Miskolc (48.3°N)	Summer	8 a.m.	ASB	13.5	15.9	~13.8 %
			CWD 45°	13.6	18.6	
			CWD 90°	13.3	**13.7**	
	Summer	12 p.m.	ASB	15.1	14.3	~9.8 %
			CWD 45°	14.8	16.0	
			CWD 90°	14.5	**12.9**	
	Winter	8 a.m.	ASB	6.1	3.3	~3.0 %
			CWD 45°	6.2	3.6	
			CWD 90°	6.2	**3.2**	
	Winter	12 p.m.	ASB	9.2	1.9	~1.0 %
			CWD 45°	9.1	2.1	
			CWD 90°	9.2	**1.88**	

deviation, often significantly worse than the conventional ASB. This is a crucial insight: while its geometry is effective for optical capture (as seen in Section 4.1), it is detrimental to thermal stability. The 45-degree concave surface acts as a more efficient lens, exacerbating the concentration of flux into a single region and creating a more intense hotspot. This highlights a fundamental design trade-off: a shape optimized for raw optical capture is not necessarily optimized for thermal management, and can in fact be counterproductive.

In summary, the quantitative data provide indisputable evidence that the CWD 90° geometry successfully and consistently homogenizes the solar flux. Its ability to reduce thermal non-uniformity, especially during periods of high insolation and at the challenging, asymmetric sun angles encountered daily, validates its potential to significantly enhance the durability and reliability of LFR receivers.

The preceding analysis has clearly established the superior flux uniformity of the CWD 90° design and the engineering trade-offs between the three geometries. To understand the underlying optical physics that drive these differences in both efficiency and flux distribution, it is necessary to deconstruct the optical performance into its constituent geometric factors. The following section analyzes the Interception Factor to reveal the fundamental mechanisms behind these results.

4.3. Interception Factor analysis

The previous sections demonstrated that the CWD 90° design provides superior thermal stability, while the CWD 45° offers modest gains in optical efficiency at low solar angles. To understand the underlying optical physics, this section analyzes the Interception Factor (IF), which measures the fraction of rays entering the secondary optic that make initial contact with the absorber surface. This analysis, summarized in Fig. 12, reveals the fundamental design trade-offs between the geometries.

4.3.1. The Interception Factor trade-off

As shown in Fig. 12, the conventional ASB design consistently achieves the highest primary Interception Factor, particularly during summer, with values reaching up to 0.83. It's simple, convex shape presents an unobstructed, convex target for the concentrated rays, making it highly efficient at initial ray capture. In contrast, the CWD designs show a slightly lower primary Interception Factor (by ~2–5 %). This is an expected geometric consequence; their concave, cavity-like structures can cause a small fraction of incoming rays to be rejected or to strike the glass envelope without first hitting the absorber. The CWD 90°, with its more extreme vertical cavity, generally shows a slightly lower primary IF than the CWD 45°. However, this simple metric of first-strike interception tells only part of the story. The key to the CWD designs' competitive performance lies not in the initial interception, but in what happens to the energy that is not immediately absorbed.

4.3.2. The cavity effect

The modest deficit in primary interception for the CWD designs is largely compensated, and in some cases overcome, by a phenomenon rooted in the principles of radiative heat transfer within non-convex enclosures, which we term the "cavity effect." From a theoretical standpoint, the concave geometry of the CWD designs increases the radiative view factor from any point on an interior surface to other interior surfaces of the absorber. Consequently, solar rays that are not absorbed upon first impact and are instead reflected (diffusely or specularly) have a high probability of striking another absorbing surface within the cavity rather than escaping back through the glass envelope to the environment.

This phenomenon effectively increases the overall effective solar absorptance of the receiver assembly. While the material's surface absorptance (α) is a fixed property (e.g., 0.92), the probability of a photon being ultimately absorbed after multiple internal reflections within the cavity approaches unity. This is analogous to the principle used to create blackbody cavities in radiometry. In contrast, for the convex ASB design, the view factor from the absorber surface to the environment is nearly 1, meaning any reflected ray is almost

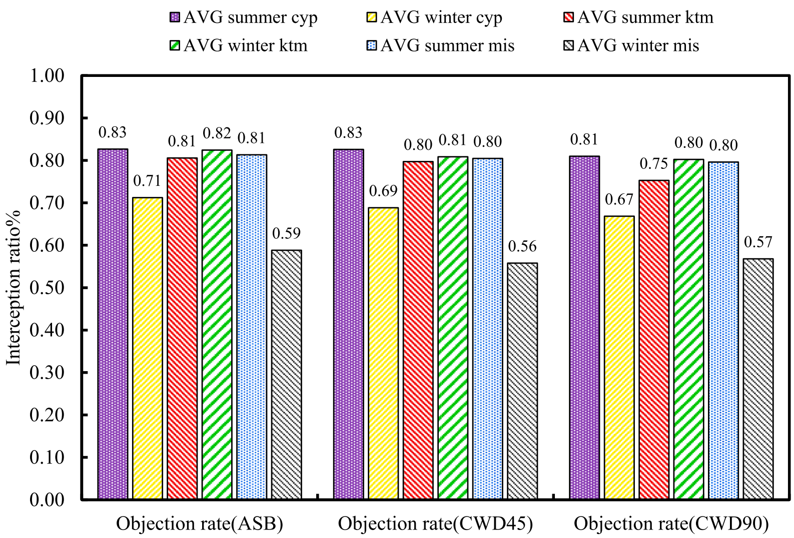

Fig. 12. Seasonal interception ratio comparison for ASB, CWD 45°, and CWD 90° absorber designs across different geographical locations."

certainly lost.

This "photon trapping" mechanism explains the key findings from our optical efficiency analysis (Section 4.1). Despite having a 2–5 % lower primary Interception Factor, the overall optical efficiency of the CWD designs is competitive with, and at low solar angles, superior to the ASB. This performance gain is a direct result of the cavity effect recovering reflected energy that would otherwise be lost, demonstrating that the energy is captured more intelligently.

5. Limitations and recommendations for future work

This study provides a comprehensive optical analysis and establishes the significant thermal management benefits of the novel CWD 90° receiver. However, to bridge the gap from optical simulation to real-world application, several limitations of the current work must be acknowledged, which in turn define clear pathways for future research.

5.1. Limitations of the current study

- The primary limitation of this research is that it is a purely optical study. It does not include a coupled thermal analysis to model heat transfer, convective and radiative heat losses, or the resulting temperature distribution on the absorber surfaces and glass envelope.
- The simulations did not consider varying environmental conditions or transient effects such as cloud cover and real-world factors like dust accumulation on optical surfaces, all of which can significantly influence long-term performance.
- The absorber geometries were treated as static. The study did not investigate the potential for dynamic adjustments or the impact of manufacturing tolerances on performance.
- The current analysis focuses on a deterministic model where material properties (reflectivity, absorptance) and geometric parameters (mirror shape, receiver position) are assumed to be perfectly known. In reality, these are subject to manufacturing tolerances, assembly errors, and degradation over time. While the ray-count convergence was validated, a comprehensive uncertainty quantification considering the statistical distributions of these real-world parameters was not performed and remains an area for future work.
- The simulations were conducted assuming perfect optical parameters (e.g., no mirror slope errors, tracking errors, or surface specularity deviations). This was a deliberate methodological choice to create a controlled simulation environment, allowing for the isolation and direct comparison of the intrinsic performance of the receiver geometries. While this approach provides a clear baseline, it does not capture the "flux blurring" effect of real-world optical errors. A future sensitivity analysis incorporating these stochastic errors is necessary to evaluate the designs' robustness under more realistic operational conditions.

5.2. Recommendations for future research

Building on these limitations, we recommend the following avenues for future investigation, categorized by discipline:

- Coupled Thermo-Fluid Dynamic Modelling: The most critical next step is to perform a comprehensive, coupled thermo-fluid dynamic analysis using Computational Fluid Dynamics (CFD). Such a study should: 1) Calculate the precise temperature distribution on the absorber walls, validating the thermal uniformity predicted by the flux maps. 2) Quantify total thermal losses (convective and radiative) from the receiver to determine the overall thermal efficiency (η_{th}). 3) Model the heat transfer to the working fluid (HTF) to determine the net useful energy output (Q_u) and outlet fluid temperature. This will provide a complete picture of the receiver's performance, from incident photons to useable heat.
- Geometric and Optical Optimization: While the CWD designs have shown great promise, their geometry is not yet fully optimized. Future work should: 1) Conduct a parametric sweep of the key geometric variables of the concave parabolic walls (e.g., focal length, rim angle) to maximize both optical capture and flux uniformity. 2) Investigate advanced non-imaging secondary optics specifically tailored to the CWD receiver's unique acceptance angle requirements to further enhance system-level efficiency.
- Techno-Economic and Life-Cycle Assessment: To justify commercial adoption, the engineering benefits must be translated into economic and environmental terms. Future research must include: 1) Life-Cycle Cost Analysis (LCCA): A detailed LCCA is needed to compare the total lifetime cost including manufacturing, installation, and reduced maintenance costs for the CWD 90° against the conventional ASB. This will determine if the improved reliability translates to a lower Levelized Cost of Energy (LCOE). 2) Life-Cycle Assessment (LCA): An LCA should be performed to evaluate the environmental impact, including the carbon footprint and resource intensity, of manufacturing and deploying these new receiver designs compared to traditional ones. 3) Manufacturability Study: A practical assessment of the manufacturing processes, challenges, and costs associated with producing the CWD profiles at scale is essential for commercial feasibility.

6. Conclusion

This research conducted a comprehensive optical evaluation of two novel Concave Wall Design (CWD 45° and CWD 90°) absorber tubes for Linear Fresnel Reflector (LFR) systems, comparing them against a conventional Absorber Standard Bore (ASB) design. Using high-fidelity Monte Carlo ray-tracing simulations for three distinct geographical locations, this study aimed to assess not only optical efficiency but also the critical, yet often overlooked, issue of heat flux uniformity and its impact on thermal stability.

The key findings of this work are as follows:

1. Optical Efficiency: While all designs demonstrated comparable peak optical efficiencies (∼0.69 %) under ideal, high-sun conditions, the CWD geometries showed a measurable advantage in capturing oblique rays. The CWD 45° design, in particular, proved to be the most optically efficient on a daily basis in mid-to-high latitudes, outperforming the ASB during crucial morning and evening hours.
2. Heat Flux Distribution and Thermal Stability: The most significant finding of this study relates to thermal management. The CWD 90° design delivered a transformative improvement in heat flux uniformity, reducing the standard deviation of the flux by 15 %–49 % compared to the ASB for lower summer sun angles and about ∼10 % for high summer sun angles. This is precisely when mitigating hotspots is most critical.

During winter, while the absolute flux and standard deviations are lower for all models due to reduced insolation, the CWD 90° still maintains its position as the most uniform design. Its percentage improvement remains substantial, particularly in Khartoum, where winter sun angles are still relatively high; the improvement in uniformity is significant, reaching 23 % compared with ASB.

3. CWD 90° with its unique geometry successfully bifurcates the concentrated solar flux, mitigating the formation of dangerous hotspots that lead to thermomechanical failure in conventional receivers. Design Trade-Offs: The study clearly delineates the critical engineering trade-offs between the designs. The ASB offers high primary ray capture but poor thermal management. The CWD 45° maximizes optical capture but at the cost of even greater thermal stress. The CWD 90° emerges as the superior balanced design, strategically sacrificing a negligible amount of primary optical performance for a substantial and crucial gain in thermal stability.
4. The study clearly delineates the critical engineering trade-offs between the designs. The ASB offers simple manufacturing and high primary optical capture but suffers from poor thermal management. The CWD 45° slightly improves optical capture at low sun angles but can exacerbate hotspots. Crucially, the CWD 90° emerges as the superior balanced design. It strategically sacrifices a negligible amount of peak optical performance (typically 1–2 %) for a substantial gain in heat flux uniformity (up to a 23 % reduction in standard deviation). This demonstrates a highly favourable trade-off, where a minor cost in energy capture yields a major benefit in the conditions governing receiver durability and lifespan.

In conclusion, this research provides compelling evidence that the novel CWD 90° receiver geometry offers a viable and highly promising solution to one of the most significant challenges facing LFR technology: receiver durability.

where that CWD 90° enhances LFR system performance by lowering peak temperatures, reducing thermomechanical stress, and minimizing thermal cycling fatigue by prioritizing uniform thermal loading, the CWD 90° design paves the way for more reliable, longer-lasting LFR systems with lower operational and maintenance costs. This work strongly supports its consideration for next-generation LFR plants where long-term economic viability and operational reliability are paramount, demonstrating that intelligent geometric design can overcome critical thermomechanical challenges inherent to the LFR concept.

CRediT authorship contribution statement

Salman Brbhan: Writing – review & editing, Writing – original draft, Visualization, Software, Methodology, Investigation, Formal analysis, Data curation. **Basim Belgasim:** Writing – review & editing, Supervision, Conceptualization. **Ahmed Al Mers:** Writing – review & editing, Validation. **Zoltán Siménfalvi:** Writing – review & editing, Supervision. **Zoltán Szamosi:** Writing – review & editing, Supervision, Resources, Funding acquisition, Data curation, Conceptualization.

Declaration of competing interest

The authors declare that they have no known competing financial interests or personal relationships that could have appeared to influence the work reported in this paper.

Acknowledgements

This paper was supported by the János Bolyai Scholarship of the Hungarian Academy of Sciences.

Appendix A. Supplementary data

Supplementary data to this article can be found online at https://doi.org/10.1016/j.csite.2025.107528.

Data availability

Data will be made available on request.

References

[1] M.I. Khan, R. Gutiérrez-Alvarez, F. Asfand, Y. Bicer, S. Sgouridis, S.G. Al-Ghamdi, H. Jouhara, M. Asif, T.A. Kurniawan, M. Abid, A. Pesyridis, M. Farooq, The economics of concentrating solar power (CSP): assessing cost competitiveness and deployment potential, Renew. Sustain. Energy Rev. 200 (2024), https://doi.org/10.1016/j.rser.2024.114551.

[2] B. Surya, A. Muhibuddin, S. Suriani, E.S. Rasyidi, B. Baharuddin, A.T. Fitriyah, H. Abubakar, Economic evaluation, use of renewable energy, and sustainable urban development mamminasata metropolitan, Indonesia, Sustainability 13 (2021) 1165, https://doi.org/10.3390/SU13031165, 13 (2021) 1165.

[3] I. Baniasad Askari, M. Ameri, A techno-economic review of multi effect desalination systems integrated with different solar thermal sources, Appl. Therm. Eng. 185 (2021), https://doi.org/10.1016/j.applthermaleng.2020.116323.

[4] A. Al-Falahi, F. Alobaid, B. Epple, Thermo-economic evaluation of aqua-ammonia solar absorption air conditioning system integrated with various collector types, Entropy 22 (2020) 1165, https://doi.org/10.3390/E22101165, 22 (2020) 1165.

[5] Q. Hassan, V.S. Tabar, A.Z. Sameen, H.M. Salman, M. Jaszczur, A review of green hydrogen production based on solar energy; techniques and methods, Energy Harvesting and Systems 11 (2024), https://doi.org/10.1515/ehs-2022-0134.

[6] A.H. Alami, A.G. Olabi, A. Mdallal, A. Rezk, A. Radwan, S.M.A. Rahman, S.K. Shah, M.A. Abdelkareem, Concentrating solar power (CSP) technologies: status and analysis, Int. J. Thermofluids 18 (2023) 100340, https://doi.org/10.1016/J.IJFT.2023.100340.

[7] D. Pulido-Iparraguirre, L. Valenzuela, J. Fernández-Reche, J. Galindo, J. Rodríguez, Design, manufacturing and characterization of linear fresnel reflector's facets, Energies 12 (2019), https://doi.org/10.3390/en12142795.

[8] E. Bellos, C. Tzivanidis, A. Papadopoulos, Secondary concentrator optimization of a linear fresnel reflector using bezier polynomial parametrization, Sol. Energy 171 (2018) 716–727, https://doi.org/10.1016/j.solener.2018.07.025.

[9] E. Bellos, C. Tzivanidis, Multi-criteria evaluation of a nanofluid-based linear fresnel solar collector, Sol. Energy 163 (2018) 200–214, https://doi.org/10.1016/j.solener.2018.02.007.

[10] S.S.L. Somda, K.E. N'Tsoukpoe, Improving optical efficiency of linear fresnel collectors in the Sahel via position and length adjustment, Solar Compass 13 (2025), https://doi.org/10.1016/j.solcom.2024.100105.

[11] M. Hack, G. Zhu, T. Wendelin, Evaluation and comparison of an adaptive method technique for improved performance of linear fresnel secondary designs, Appl. Energy 208 (2017) 1441–1451, https://doi.org/10.1016/j.apenergy.2017.09.009.

[12] M. Imran Khan, F. Asfand, S.G. Al-Ghamdi, Progress in research and technological advancements of commercial concentrated solar thermal power plants, Sol. Energy 249 (2023) 183–226, https://doi.org/10.1016/j.solener.2022.10.041.

[13] M.J. Montes, R. Abbas, M. Muñoz, J. Muñoz-Antón, J.M. Martínez-Val, Advances in the linear Fresnel single-tube receivers: hybrid loops with non-evacuated and evacuated receivers, Energy Convers. Manag. 149 (2017) 318–333, https://doi.org/10.1016/j.enconman.2017.07.031.

[14] M.A. Moghimi, K.J. Craig, J.P. Meyer, A novel computational approach to combine the optical and thermal modelling of Linear Fresnel Collectors using the finite volume method, Sol. Energy 116 (2015) 407–427, https://doi.org/10.1016/j.solener.2015.04.014.

[15] N.D. Kaushika, K. Sumathy, Solar transparent insulation materials: a review, Renew. Sustain. Energy Rev. 7 (2003) 317–351, https://doi.org/10.1016/S1364-0321(03)00067-4.

[16] A.C. Montenon, N. Fylaktos, F. Montagnino, F. Paredes, C.N. Papanicolas, Concentrated solar power in the built environment, in: AIP Conf Proc, American Institute of Physics Inc., 2017, https://doi.org/10.1063/1.4984402.

[17] A.C. Montenon, A.V. Santos, M. Collares-Pereira, F.M. Montagnino, R. Garofalo, C. Papanicolas, Optical performance comparison of two receiver configurations for medium temperature Linear Fresnel Collectors, Sol. Energy 240 (2022) 225–236, https://doi.org/10.1016/j.solener.2022.05.029.

[18] E. Bellos, Progress in the design and the applications of linear Fresnel reflectors – a critical review, Therm. Sci. Eng. Prog. 10 (2019) 112–137, https://doi.org/10.1016/j.tsep.2019.01.014.

[19] M.A. Moghimi, K.J. Craig, J.P. Meyer, Optimization of a trapezoidal cavity absorber for the Linear Fresnel Reflector, Sol. Energy 119 (2015) 343–361, https://doi.org/10.1016/j.solener.2015.07.009.

[20] Introduction to NONIMAGING OPTICS. https://doi.org/10.1201/b18785, 2017.

[21] H. Hoseinzadeh, A. Kasaeian, M. Behshad Shafii, Geometric optimization of parabolic trough solar collector based on the local concentration ratio using the Monte Carlo method, Energy Convers. Manag. 175 (2018) 278–287, https://doi.org/10.1016/j.enconman.2018.09.001.

[22] I. Bouarfa, M. El Ydrissi, H. El Hafdaoui, M. Boujoudar, A. Jamil, E.G. Bennouna, Developing optical and thermal models with experimental validation of parabolic trough collector for moroccan industrial heat applications, Sol. Energy Mater. Sol. Cell. 266 (2024), https://doi.org/10.1016/j.solmat.2023.112676.

[23] M.J. Blanco, V. Grigoriev, K. Milidonis, G. Tsouloupas, M. Larrañeta, M. Silva, Minimizing the computational effort to optimize solar concentrators with the open-source tools sunpath and tonatiuh++, Energies 14 (2021) https://doi.org/10.3390/en14154412.

[24] D. Jafrancesco, J.P. Cardoso, A. Mutuberria, E. Leonardi, I. Les, P. Sansoni, F. Francini, D. Fontani, Optical simulation of a central receiver system: comparison of different software tools, Renew. Sustain. Energy Rev. 94 (2018) 792–803, https://doi.org/10.1016/j.rser.2018.06.028.

[25] O. Chakraborty, S. Nath, Numerical study on solar trough collectors: optimizing heat transfer with ternary nanoparticles in ionic base fluid and spinning tube fins, Renew. Energy 236 (2024), https://doi.org/10.1016/j.renene.2024.121473.

[26] D.N. Korres, T. Papingiotis, I.P. Koronaki, C. Tzivanidis, Experimental analysis and optimization of a concentrated thermo-photovoltaic collector with bi-facial receiver, Renew. Energy 236 (2024), https://doi.org/10.1016/j.renene.2024.121401.

[27] N. Stsepuro, M. Kovalev, I. Podlesnykh, S. Kudryashov, A new approach to designing multi-element planar solar concentrators: geometry optimization for high angular selectivity and efficient solar energy collection, Optics 6 (2025), https://doi.org/10.3390/opt6010006.

[28] F. Masood, N.B.M. Nor, I. Elamvazuthi, R. Saidur, M.A. Alam, J. Akhter, M. Yusuf, S.M. Ali, M. Sattar, M. Baba, The compound parabolic concentrators for solar photovoltaic applications: opportunities and challenges, Energy Rep. 8 (2022) 13558–13584, https://doi.org/10.1016/j.egyr.2022.10.018.

[29] M.J. Blanco, M.J. Blanco, A. Mutuberria, P. Garcia, R. Gastesi, V. Martin, Preliminary validation of Tonatiuh. https://www.researchgate.net/publication/212165994, 2009.

[30] A.C. Montenon, P. Tsekouras, C. Tzivanidis, M. Bibron, C. Papanicolas, Thermo-optical modelling of the linear Fresnel collector at the Cyprus institute, in: AIP Conf Proc, American Institute of Physics Inc., 2019, https://doi.org/10.1063/1.5117613.

[31] J.M. García-Moreno, A.C. Montenon, M.A. Nicolaou, W. Lipiński, K. Milidonis, Artificial intelligence-aided generative design of non-imaging secondary reflector for linear Fresnel concentrating collector, Sol. Energy 292 (2025), https://doi.org/10.1016/j.solener.2025.113415.

[32] A. Fernández-García, E. Zarza, L. Valenzuela, M. Pérez, Parabolic-trough solar collectors and their applications, Renew. Sustain. Energy Rev. 14 (2010) 1695–1721, https://doi.org/10.1016/j.rser.2010.03.012.

[33] S. Balaji, K.S. Reddy, T. Sundararajan, Optical modelling and performance analysis of a solar LFR receiver system with parabolic and involute secondary reflectors, Appl. Energy 179 (2016) 1138–1151, https://doi.org/10.1016/j.apenergy.2016.07.082.

[34] J.A. Duffie, W.A. Beckman, Frontmatter, in: Solar Engineering of Thermal Processes, Wiley, 2013, https://doi.org/10.1002/9781118671603.fmatter.

[35] D. Pulido-Iparraguirre, L. Valenzuela, J.J. Serrano-Aguilera, A. Fernández-García, Optimized design of a Linear Fresnel reflector for solar process heat applications, Renew. Energy 131 (2019) 1089–1106, https://doi.org/10.1016/j.renene.2018.08.018.
[36] O. Achahour, B. El Ghazzani, R. Safoui, A. Eddemani, M. Abbassi, A. Elfanaoui, A. Ihlal, Experimental investigation on Linear fresnel reflector prototype for SolaHeat production, Renewable Energy and Sustainable Development 11 (2025) 146–161, https://doi.org/10.21622/resd.2025.11.1.1277.
[37] H. Wang, J. Huang, M. Song, J. Yan, Effects of receiver parameters on the optical performance of a fixed-focus Fresnel lens solar concentrator/cavity receiver system in solar cooker, Appl. Energy 237 (2019) 70–82, https://doi.org/10.1016/j.apenergy.2018.12.092.